

Strategic Astrophysics Technology

Milestone #1 Final Report

Linear Wavefront Control

June 25, 2021

Olivier Guyon, P.I.

Thayne Currie, Ruslan Belikov, Eugene Pluzhnik, Tyler D. Groff, Julien Lozi

Charlotte Bond, Mark Chun, Richard Frazin, Brian Kern, Jared Males, Ben Mazin, Bijan Nemati,
Dan Sirbu, Hari Subedi, Kelsey Miller, Steven Bos, Barnaby Norris

Signature Page

Olivier Guyon, Principal Investigator

Date

Nick Siegler (ExEP Program Chief Technologist)

Date

Exoplanet Exploration Program, NASA / JPL - California Institute of Technology

Brendan Crill (Deputy ExEP Program Chief Technologist)

Date

Exoplanet Exploration Program, NASA / JPL - California Institute of Technology

Doug Hudgins

Date

ExEP Program Scientist NASA-HQ

Table of Contents

1. Executive Summary.....	3
2. SAT Description.....	4
3. Milestone.....	9
4. Conclusions.....	13
5. References.....	17

Executive Summary

The milestone completion described in this document is part of the NASA-funded effort “Linear Wavefront Control for High Contrast Imaging”, which is aimed at improving the efficiency, sensitivity, and reliability of wavefront control for exoplanet imaging.

Imaging planets in reflected light, a key focus of future NASA missions, requires advanced wavefront control to maintain a deep, temporally correlated null of stellar halo -- i.e. a dark hole -- at just several diffraction beam widths. Linear Dark Field Control (LDFC) is a wavefront stabilization approach making use of bright starlight to stabilize a deep null in a coronagraphic image. LDFC uses the response to perturbations in uncorrected, 'bright field' regions to maintain a dark hole without continuous DM probing.

Results presented in this document are aimed at completing LDFC milestone #1 (MS1) defined in the LDFC Milestone #1 white paper:

“Demonstrate a 10x gain in raw contrast in the presence of injected disturbances by use of LDFC stabilization in a dark hole with area covering at least 10 square- λ/D and reaching a raw contrast level below $1e-5$.”

We reached and exceeded this milestone using the Ames Coronagraph Experiment testbed conducting the first laboratory tests of Spatial Linear Dark Field Control (LDFC). These tests were carried out at raw contrasts ($\cong 5e-7$) and separations (1.5--5.2 λ/D)

approaching those needed to image jovian planets around Sun-like stars with space-borne coronagraphs like Roman-CGI and image exo-Earths around low-mass stars with future ground-based 30m class telescopes.

In four separate experiments, we perturb the initial dark hole using a range of different phase perturbations, reducing the contrast within a > 10 squared- λ/D scoring region by a factor of 11-26. LDFC demonstrates a factor of $>10x$ gain in contrast within this scoring region, largely restoring (to within a factor of 1.2--1.7) the original dark hole intensity. The correction is stable: LDFC maintains it for over 100 iterations. Our implementation of classical speckle nulling requires a factor of 2--5 more iterations and 20--50 DM commands to reach contrasts obtained by spatial LDFC. Our results provide a promising path forward to maintaining dark holes without relying on DM probing and in the low-flux regime, which may improve the duty cycle of high-contrast imaging instruments, increase the temporal correlation of speckles, and thus enhance our ability to image true solar system analogues in the next two decades. Results have also been compiled in a refereed paper (Currie et al. 2020) provided as an attachment to this document.

SAT Description

Background and Motivation

Over the past decade, ground-based telescopes using facility adaptive optics (AO) systems and now dedicated *extreme* AO systems have provided the first direct images of (super-)jovian mass planets in thermal emission orbiting young stars (e.g. Marois et al. 2008). Imaging exoplanets in reflected light from future space missions or ground-based extreme AO systems requires factors of 100-1000 gains in contrast and thus new advances in wavefront control (WFC) and coronagraphy (e.g. Guyon et al. 2018c; Crill et al. 2019).

Advances in the laboratory and on sky have made significant progress towards achieving the performance necessary to detect reflected-light planets. High-contrast imaging testbeds utilizing focal plane WFC techniques like speckle nulling and electric field conjugation (EFC) and advanced coronagraphy can generate deep dark holes (DH) around a star at the 10^{-9} level or lower in vacuum (e.g. Borde et al. 2006; Give'on et al. 2007; Cady et al. 2016). On ground-based telescopes, wavefront sensing and control advances (e.g. Zernike phase sensing and predictive control) have shown promise on new, state-of-the-art extreme AO systems like SCExAO and could yield orders of magnitude gain in raw contrast (N'diaye et al. 2016, Males and Guyon 2018).

Sustaining deep contrasts within a DH necessary to image planets in reflected light imposes significant demands on wavefront sensing, as the residual stellar halo must be measured with extreme precision. Precision sensing is particularly difficult when the

DH itself is used for focal-plane wavefront control (FPWFC) and is already photon starved, as can be the case for standard methods like EFC and speckle nulling. Furthermore, by modulating the deformable mirror (DM) to determine and update an estimate of the electric field, FPWFC methods like EFC can perturb science exposures and thus limit an observation's duty cycle. Instead of using the science target for FPWFC itself, another strategy (for Roman CGI) is to first dig a DH around a far brighter reference star within 15-20 degrees of a science target and then apply the high-order DM correction to the science target (Bailey et al. 2018). However, both the average contrast of the DH and its temporal correlation with respect to its initial state can and likely will degrade due to any number of dynamic aberrations. Slewing back to the reference star to rebuild the DH, as is currently baselined for CGI, substantially increases an observation's duty cycle. Advanced post-processing methods can yield substantial contrast gains (e.g. Soummer et al. 2012) But the brightening of the DH and its decorrelation over time degrades the effectiveness of these post-processing methods to remove residual starlight impeding planet detection.

Linear Dark Field Control (LDFC) is a promising wavefront control method which could maintain a static, deep DH without deformable mirror probing after the DH's creation from FPWFC methods (Miller et al. 2017; Figure 1). LDFC utilizes the linear response of the uncorrected but photon-rich region in the focal plane (the "bright field" or BF) to wavefront perturbations that affect both the BF and the photon-starved DF. Because LDFC does not require modulating the signal within the DH, it needs only a single focal plane image to restore the electric field to its initial state.

LDFC is a wavefront stabilization technique, but is not suitable to iteratively build a dark hole like EFC or speckle nulling. Therefore the two approaches would be used sequentially or in parallel. Once a dark hole is established through FPWFC methods, LDFC may be used as the sole control loop, or can run in addition to other control loop(s).

The technique's strengths and limitations are listed below, compared to the better established DM probing approaches.

LDFC strengths

- **Sensitivity:** LDFC can use more light than available within the spatial and spectral extent of the dark hole, resulting in improved sensitivity
- **DM probing-free:** Since no DM perturbations are required for the loop to operate, science acquisitions can be done at full duty cycle.
- **Ease of calibration:** As LDFC is a linear control technique (LDFC-requ1), it uses derivatives of the pixel intensities relative to DM actuation for calibration. This calibration can be measured by DM probing in a reasonably short amount of time, so the technique is not as sensitive to modeling errors as EFC-like approaches that require a numerical model of the coronagraph system.
- **Linearity:** The linear control loop is fast to execute, and common linear analysis techniques can be deployed for optimization and analysis.

- **Scalability:** Multiple sensors (cameras at multiple wavelengths) can easily be integrated in a LDFC control scheme, as no dark hole is required and no DM probing is required.

LDFC limitations

- LDFC is a **differential** sensing technique that cannot by itself drive the system to a high contrast state. It is only a wavefront stabilization technique.
- A **null space** may exist: not all wavefront modes can be sensed, and some of the unseen modes can negatively impact contrast.
- **Non-stationarity** of the relationship between bright field, wavefront state and dark hole illumination can build up over time.

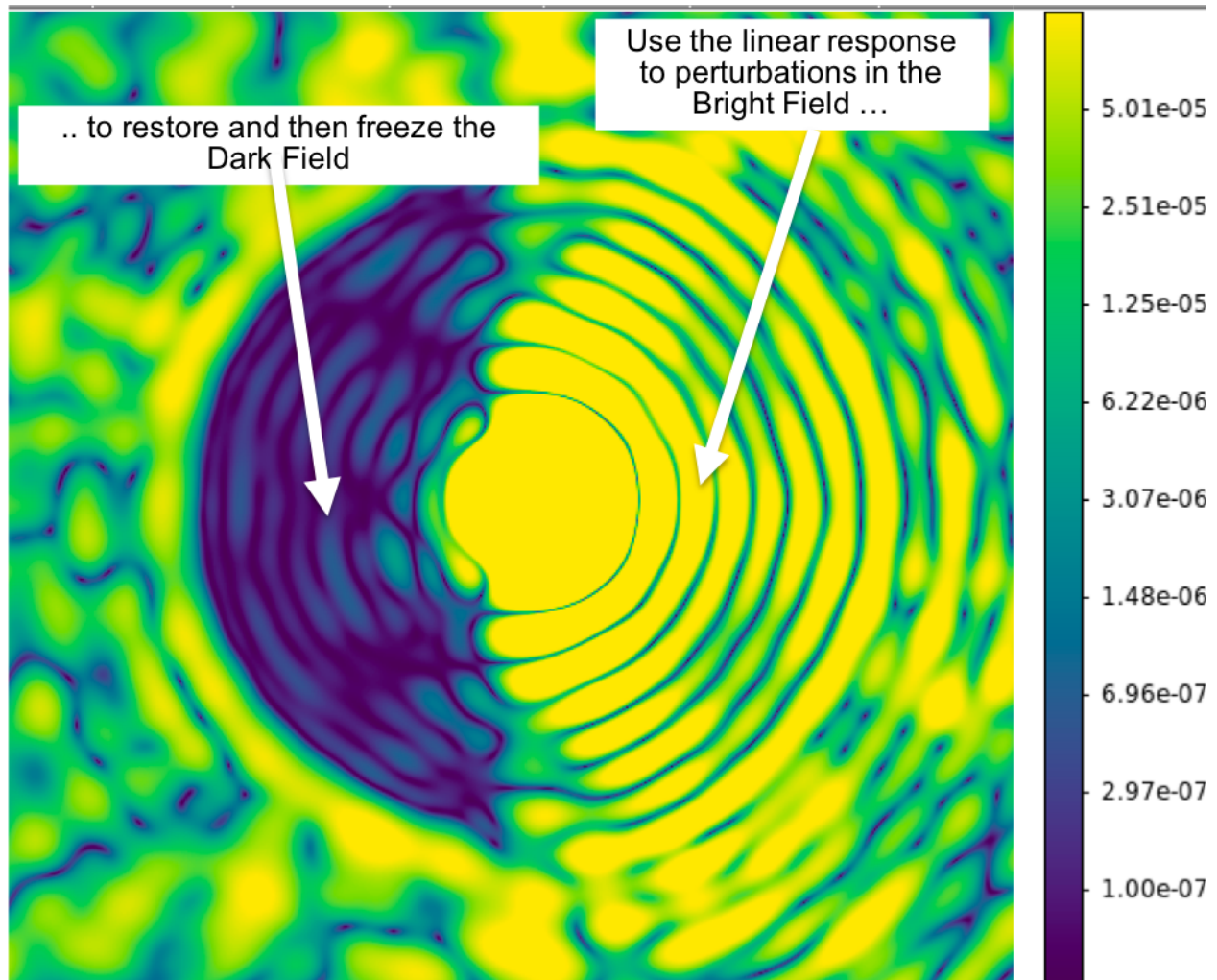


Figure 1: Schematic of Spatial Linear Field Dark Control obtained from simulated data for the Ames Coronagraph Experiment testbed. Bright, uncorrected regions with a contrast with respect to the peak intensity of 10^{-4} are used to stabilize a dark hole with a contrast of $\sim 10^{-7}$ - 10^{-8} . The dark hole region is of roughly similar scale to those used in our experiments (~ 1.5 — $5.1 \lambda/D$).

LDFC can be implemented in at least two ways. **Spatial LDFC** in a single band image, where a DH is created on one side of the image and stabilized by the BF on the opposite side (Miller et al. 2017) as shown in Figure 1. **Spectral LDFC** where the BF draws from pixels in out-of-band image slices at wavelengths bracketing the bandpass within which the DH is created (Guyon et al. 2017).

Our NASA-funded SAT effort is aimed at validating both spatial and spectral LDFC. This document presents results for Milestone 1 (MS 1), which was formulated in the MS1 whitepaper, and focuses on spatial LDFC. Future milestones and demonstrations will validate spectral LDFC and also explore system-level LDFC operation in realistic conditions to improve the approach technology readiness level (TRL).

Experimental Overview: Laboratory Setup

We conducted tests of LDFC using the Ames Coronagraph Experiment (ACE) laboratory at NASA-Ames Research Center in four separate experiments between September 2019 and January 2020 (Table 1) at contrast levels shallow enough that phase errors are expected to dominate but deep enough to be relevant for future ground and space high-contrast imaging.

The testbed uses a laser centered on 635nm as a monochromatic light source. To limit file size and improve the speed of the wavefront control loop, we readout focal-plane images in subarrays of 500x500 or 700x700 pixels. The $1\lambda/D$ full-width-at-half-maximum point-spread function (PSF) size measured ~ 32 pixels. For each experiment, satellite speckles were used to determine the conversion factor between counts and contrast with respect to the peak of an unocculted PSF. We used the PIAA coronagraph to suppress scattered starlight (Guyon et al. 2010) and a circular focal plane occulting spot of $\sim 1\lambda/D$ radius to yield a full 360 degree spatial coverage.

Experiment Number	Date	Dark Field Size (λ/D)	Bright Field Size (λ/D)	Starting Dark Hole Contrast	Scoring Region Area	Starting Dark Hole Contrast (Scoring Region)	Aberrated Dark Hole Contrast (Scoring Region)	Improvement Factor (Scoring Region)	Aberrations
1	2019-09-19	1.6-5.1	1.4-5.1	6.60×10^{-7}	$37 (\lambda/D)^2$	6.60×10^{-7}	7.02×10^{-6}	8.5 ^a	Single speckle
2	2019-12-23	1.6-5.1	1.6-5.1	5.97×10^{-7}	$10 (\lambda/D)^2$	5.46×10^{-7}	7.24×10^{-6}	9.8	Two speckles
3	2020-01-12	1.65-5.2	1.55-5.2	6.85×10^{-7}	$10 (\lambda/D)^2$	5.94×10^{-7}	9.55×10^{-6}	12	Low spatial frequency
4	2020-01-25	1.65-5.2	1.65-5.2	4.97×10^{-7}	Hemisphere $19 (\lambda/D)^2$	4.6×10^{-7}	1.20×10^{-5}	13.2	Complex, three speckles

Table 1. Experiment Log. Notes: a) The improvement in the hemisphere with the imputed speckle is a factor of ~ 100 .

To achieve an initial flat wave-front at the pupil plane, we use an implementation of the Gerchberg-Saxton method, which solves for the flat DM shape using a sequence of random pupil plane phase probes (Pluzhnik et al. 2017). Following previous ACE experiments (e.g. Belikov et al. 2012), we used a classical speckle nulling control loop to correct for up to 81 speckles at a time. For each iteration of speckle nulling, we issue on average 10 DM commands to solve for the speckles' phases and amplitudes.

The speckle nulling loop created a one sided, C-shaped DH extending from an inner working angle of 1.5–1.6 λ/D to an outer working angle of 5.1–5.2 λ/D . The average contrast within the DH measured between 4.97×10^{-7} and 6.85×10^{-7} depending on the experiment. In units of contrast, the approximate read-noise level of the detector was $\sim 5 \times 10^{-7}$ for the September and December experiments and a factor of 2 lower for the January experiments due to a factor of ≈ 10 longer exposures for the latter. Assuming a reasonable gain from post-processing (e.g. 30-50x), these raw contrasts are similar to the performance needed to detect jovian planets at ~ 1 au in reflected light around nearby stars.

Experimental Overview: LDFC Wavefront Control Loop

Miller et al. (2017) give an overview of LDFC theory. Briefly, spatial LDFC works by 1) measuring changes in the bright field intensity between time t_0 when the DH is first established and time t where it is corrupted and 2) constructing an influence function mapping between DM shape and focal plane intensity, one can then determine the set of DM actuator offsets that restore both the initial bright field and initial dark field corrupted by phase errors.

For an influence function, we adopt a system response matrix, RM , with dimensions of n bright field pixels by m actuators. The RM links together changes in DM shape Δu_t to changes in the bright field intensity distribution: $\Delta I_{DM,t} = RM \Delta u_t$. Actuator offsets Δu_t required to drive the dark field back to its original state at time t are then equal to the pseudo-inverse of RM (i.e. the “control matrix”, CM) multiplied by the change in the brightfield, ΔI_{BF} :

$$\Delta u_t = -CM \Delta I_{t,BF}. \quad (1a)$$

$$CM = (RM^T RM)^{-1} RM^T \quad (1b)$$

To calculate the Spatial LDFC RM , we followed a simplified version of methods outlined in the CACAO software used for SCAExAO and perturbed each of the m actuators by a series of small amplitude pokes, 1 and 2, which are performed sequentially and have

opposite signs (positive and negative). We then recorded the intensity I over n BF pixels. Each of the pokes have a fixed amplitude of $ampl_{poke}$. We combine results from two separate patterns $-a$ and b —which differ by the order in which the positive/negative pokes are applied (i.e. $a = +- +- , b = +- -+$):

$$RM(n,m) = 0.5*[(I_{a1}-I_{a2})+(I_{b1}-I_{b2})]/(2*ampl_{poke}). \quad (2)$$

The response matrix (RM) was acquired immediately after a dark hole was established by speckle control, with an average intensity equal to the value quoted in table 1. The RM acquisition was time consuming, so the contrast value was measured upon completion of the RM acquisition. If contrast had drifted above the pre-RM value, a few additional iterations of speckle nulling were performed to recover the pre-RM value.

We apply truncated singular value decomposition (SVD) regulation to compute the CM as the pseudo-inverse of the RM , decomposing $(RM^T RM)^{-1}$ into a matrix of eigenvectors V and a matrix of eigenvalues Λ , truncating Λ at mode k_{lim} before inverting to yield $CM = (V \Lambda^{-1} V^T)_{k < k_{lim}} RM^T$.

We determined the appropriate modal cutoff experimentally, analyzing the normalized singular values of the RM covariance as a function of mode and visually inspected the modal response. The normalized values decline to 10^{-3} by $k=200$ and flatten to 10^{-4} between $k=250$ and $k=1024$. We set the modal cutoff to the CM at $k = 250$, as modes up to this number are still dominated by spatially-correlated signal.

The $k=250$ modal cutoff choice was empirically derived by open-loop tests prior to close-loop LDFC operation. A static aberration was injected, with the initial pre-aberration and aberrated dark hole intensity images recorded along with the bright field images and DM command to produce the aberration. The CM and LDFC command were computed for a range of k -values, and the corresponding post-LDFC correction dark hole recorded. We observed contrast improvement as k increases to ~ 250 , and onset of instability with $k > 250$.

Our closed-loop implementation of LDFC multiplies the DM offset shape in the i -th iteration $\Delta u_{t,i}$ by a gain g and adds this value to the current DM shape: $DM_i = DM_{i-1} + \Delta u_{t,i} \times g$. We tested a range of gain values. For simplicity, we set $g=0.25$ for all experiments, since it provided a good balance between convergence speed and stability.

Environmental Effects

Each command to send a DM shape and then receive the corresponding wavefront sensor image took between about 5 and 20 seconds, a length duration largely due to the ACE file transfer setup and NASA-Ames Information Technology restrictions. Each

full iteration of LDFC – initial image, new DM shape determination, and new (corrected) image) -- took between about 30 and 120s.

Early tests showed that the laser light source within ACE exhibited long-term centroid drift on a timescale comparable to our *RM* collection and closed-loop tests. Thus, the laser centroid position could be different between the response matrix measurement (i.e. the influence function) and its implementation in the spatial LDFC closed loop. To monitor and correct (within 1 pixel) the estimate of the centroid position, we introduced a single speckle into the darkhole prior to compare the centroid position at the start of the RM calculation and that during closed-loop tests, shifting the bright and dark field pixel masks by the offset between these two centroid measurements. Typical offsets were on the order of 2–4 pixels ($0.06\text{--}0.12\lambda/D$); typical drift during closed-loop tests described below was on order of ~1–2 pixels.

Milestone

The experimental setup and methods described above are designed to meet SAT milestones. Completion of this milestone is documented in this report and reviewed by the Exoplanet Exploration Program. For this report, we are tasked with completing a single Milestone (Milestone #1).

Milestone Definition

Our Linear Dark Field Control Milestone #1 (MS1) is defined as follows:

Demonstrate that wavefront stabilization by LDFC achieves at least a 10x gain in raw contrast in the presence of dynamic wavefront aberrations. The contrast gain shall be measured over a focal plane area covering at least 10 sq λ/D , and at a raw contrast (post-LDFC) below $1e-5$.

Successful demonstration of LDFC also required the following:

- Stability. Quantitatively, we required that LDFC's contrast gain be demonstrated for 100 successive iterations of the wavefront control loop. Thus, after LDFC reached its nominal contrast floor after correcting for aberrations, we continued to monitor the average dark hole intensity and average intensity within the evaluation region for at least 100 additional iterations.
- Repeatability. We required three successful, independent tests of LDFC's contrast gain. Success criteria were the same in each case, based on the average contrast within a 10 sq λ/D region within the dark hole. To satisfy "independent", we conducted the tests on different dates. In each case, the dark hole was generated anew from a flat DM state via speckle nulling.

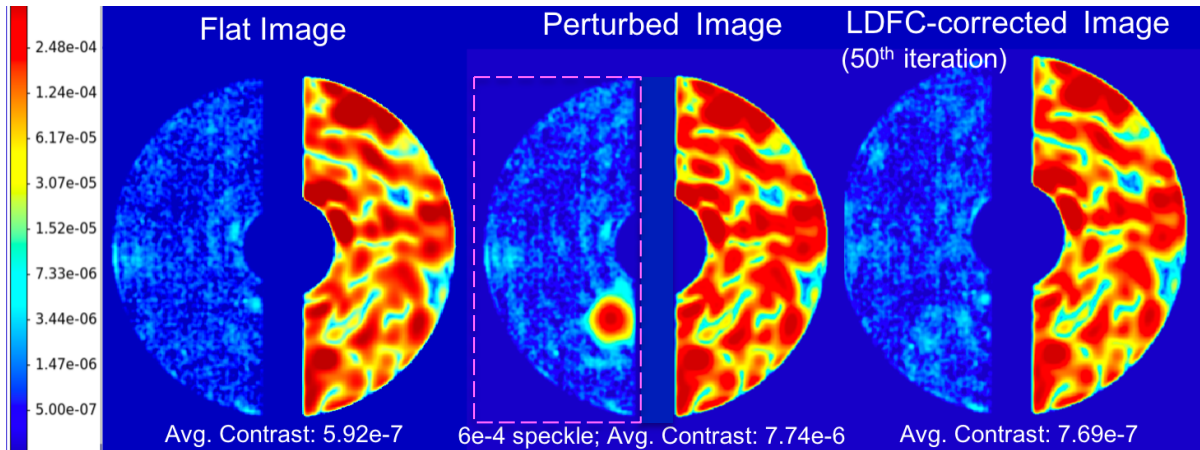


Figure 2 - Sequence of focal plane camera images from our 19 September 2019/ "Single Speckle" experiment showing that LDFC removes a bright speckle and drives the dark field back to an average contrast within 30% of its original value. The spatial scale for the dark (left) and bright (right) field regions is given in Table 1 and is roughly 1.5--5.1 λ/D ; regions outside this range are masked out. The scoring region is the union of the half-dark hole and the box outlined in magenta (middle panel).

Detailed Test Results

Figures 2--5 display the main results of our experiments, demonstrating the ability of Spatial LDFC to restore a DH corrupted by a range of different phase-induced aberrations: one bright speckle, two speckles, a broad low spatial frequency aberration, and three speckles. The September 2019 experiment (Experiment #1) provides a simple demonstration. Here, an initial ('flat') image with an average DH contrast of 6.6×10^{-7} is degraded by a single speckle with a peak contrast that is a factor of 1000 larger ($\sim 6.4 \times 10^{-4}$), yielding an average intensity within the DH of $\sim 7.0 \times 10^{-6}$, increasing the average contrast over the entire DH by a factor of ~ 11 in the presence of this aberration. Spatial LDFC immediately begins removing this speckle. LDFC achieves a restored DH with a contrast within $\sim 20\%$ of the original DH average intensity, nearly a factor of 10 gain in contrast over the entire hemisphere and much, much greater over the half of the DH containing the speckle.

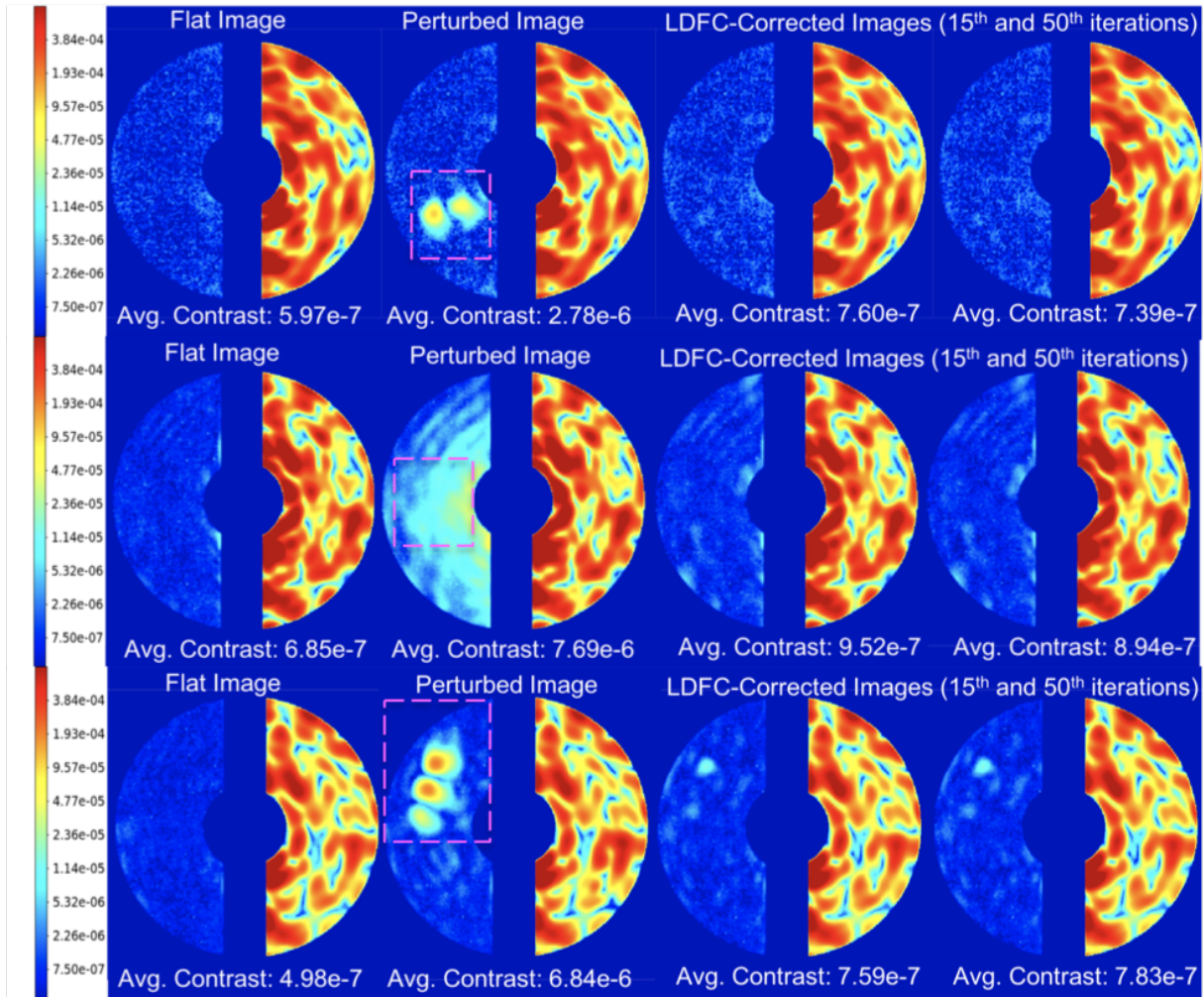


Figure 3 - Sequence of images for Linear Dark Field Control experiments conducted on 23 December 2019 "Pair of Speckles" (top row), 12 January 2020 "Low Spatial Frequency Aberration" (middle row), and 25 January 2020 "Complex Aberration" experiments (bottom row). Shown are the initial camera image after the creation of a dark hole (left), the camera image after the introduction of a perturbation that degrades the dark hole (middle-left), and images after the 15th and 50th iteration of Linear Dark Field Control (middle-right, right). The spatial scale is the same as in Figure 2: the dark hole (lefthand hemisphere) covers ~ 1.6 – $5.1 \lambda/D$. Even for strong perturbations degrading contrast by over an order of magnitude, LDFC still returns the average intensity of the dark hole to within 20-40% of its original value. Dashed magenta boxes show the scoring region for each experiment.

The three experiments carried out in December 2019 and January 2020 directly fulfill our milestone requirements. The initial DH contrasts range between 5 and 6.9×10^{-7} over the entire DH and 4.6 – 5.9×10^{-7} within the relevant scoring regions. Aberrations degrade the average DH intensity by a factor of 4.6 – 13.7 ; within the scoring regions, the DH contrast is made 13 – 26 times brighter to $C \sim 7.2 \times 10^{-6}$ – 1.2×10^{-5} .

Spatial LDFC then reduces the aberrated DH contrast by a factor of 3.7--9 over the entire field ($7.4\text{--}9.5\times 10^{-7}$) and a factor of 10--13 over the scoring regions ($7.4\text{--}9.1\times 10^{-7}$). Over the entire DH region, LDFC reaches an average contrast within a factor of 1.2--1.4 of the pre-aberrated state. Within the scoring region, the restored average contrast is within a factor of 1.2--1.97 of its original value.

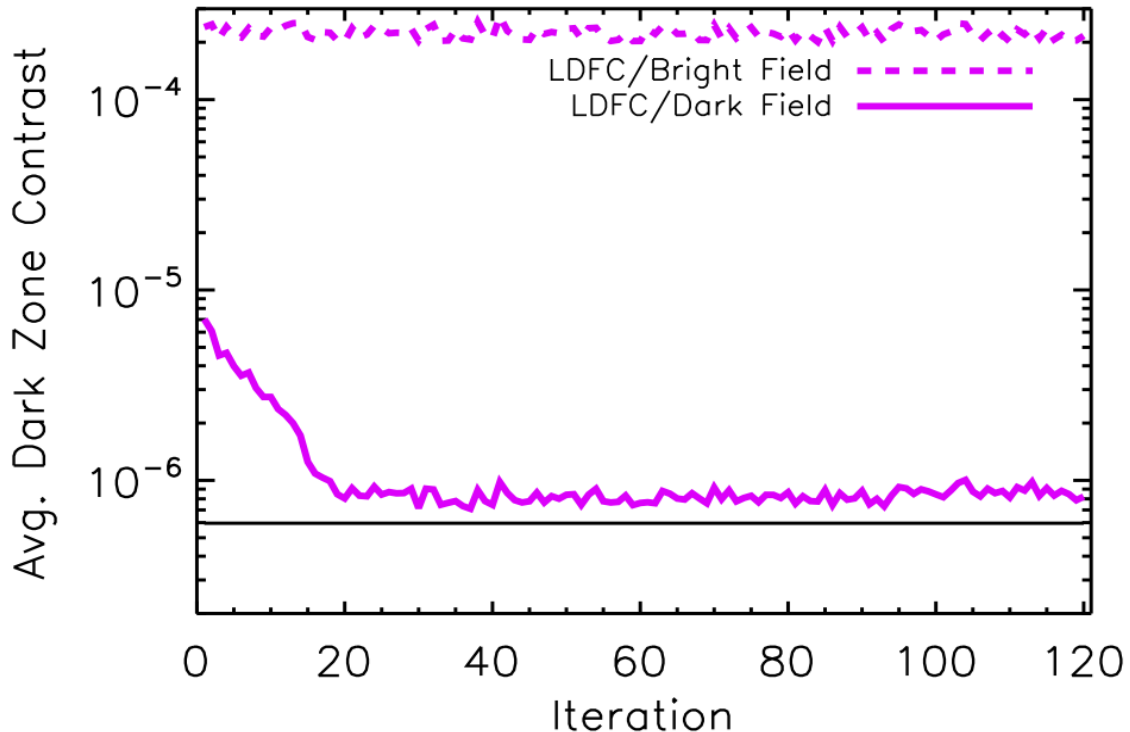


Figure 4 - Analysis of our 19 September 2019 "Single Speckle" experiment. Contrast per iteration for LDFC for the perturbation introduced in Figure 2, showing that LDFC sustains a dark hole below 10^{-6} contrast for over 100 consecutive iterations.

For Experiments 1--3, the initial aberration is (almost) perfectly removed by LDFC and most residual left by LDFC is largely confined to the edges of the DH region. We speculate that LDFC does not fully remove residual signal because a) regions near the edge of the dark field/bright field are generally more difficult to correct and b) the correction becomes 'noisier' as average contrast approaches the read noise level.

For Experiment #4, the initial aberration is largely removed but a faint residual core (~ 7 pixels in radius) of the brightest speckle remains after LDFC at a 10^{-5} level. This could be due to part of the aberrations being within the measurement null space: a fraction of the disturbance introduced on the DM does not create a BF intensity modulation, so it is not corrected.

The Spatial LDFC-restored DH shows long-term stability. For the September experiment, the DH contrast converges after 18 iterations to a value of $8 \times 10^{-7} \pm 6.5 \times 10^{-8}$ for the next 105 iterations (Figure 4). The bright field stays constant within

about the same fractional value: the average intensity fluctuations are expected given measured variations of the laser brightness with time (~5%). For the December and January experiments (Figure 5), convergence to a final (largely-)restored DH occurs within 5-10 iterations and stays constant within 10% for 110 iterations.

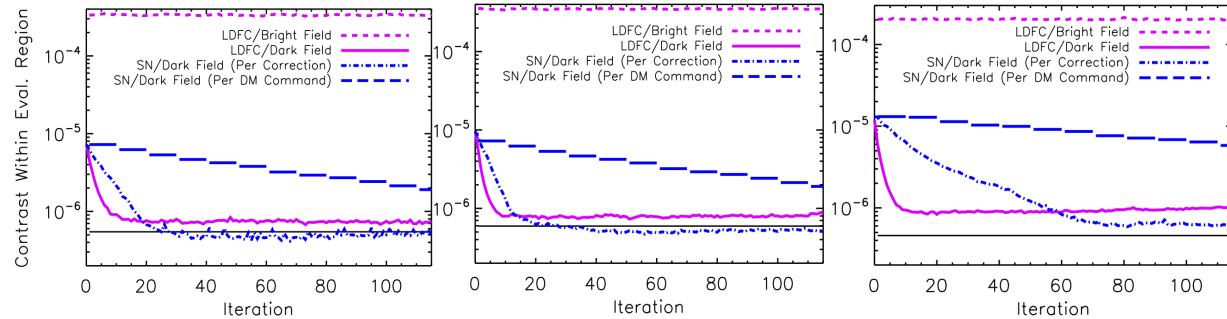


Figure 5 - Contrast per iteration for the 23 December 2019/"Pair of Speckles" (left), 12 January 2020/"Low Spatial Frequency Aberration" (middle), and 25 January 2020/"Complex Aberration" (right) experiments for Linear Dark Field Control compared to performance of the speckle nulling (SN) algorithm used to create the dark hole. Horizontal black lines denote the initial average contrast within the evaluation region before a perturbation is introduced to degrade the dark hole by a factor of 10-12. Within the dark hole, LDFC (solid magenta line) converges to within 20-40% contrast twice as fast as deformable mirror probing with speckle nulling (blue dot-dashed line) and with a factor of 20 or fewer deformable mirror commands (blue long-dashed line).

LDFC shows evidence for significantly improved efficiency compared to DM probing methods like speckle nulling. Speckle nulling is able to restore the DH to a contrast level $\sim 5\text{--}6 \times 10^{-7}$: 25--40% lower than LDFC and comparable to the initial, unperturbed DH contrast. However, speckle nulling requires 20--70 iterations to reach its final contrast level (dash-dotted blue lines). Reaching the contrast level achieved by LDFC requires a factor of 2--5 more iterations.

When analyzed in terms of DM commands, the efficiency advantage of LDFC is significantly larger. For each iteration, speckle nulling requires multiple DM probes in order to estimate the phase of residual speckles in the dark zone and estimate amplitude: 10 for our implementation. Speckle nulling requires a factor of 20--50 more DM commands to reach the contrasts achieved by LDFC. The advantage in duty cycle is particularly large for complex aberrations introduced into the focal plane (Experiment 4).

Conclusions

Summary of Results

This report presents a successful completion of Milestone 1 of our Strategic Astrophysics Technology program on *Linear Wavefront Control*. Milestone 1 focused on a demonstration of Spatial Linear Dark Field Control below 10^{-5} contrast levels or

below, requiring that Spatial LDFC yield a contrast gain in the Dark Hole by a least a factor of 10 after it had been degraded by perturbations introduced into the focal plane.

Our experiments exceed these requirements. We provide the first laboratory demonstrations of Spatial LDFC at contrast levels ($\sim 5 \times 10^{-7}$) and separations (~ 1.2 -- $5.2 \lambda/D$) approaching the raw performance needed to image some jovian planets in reflected light around the nearest Sun-like stars with space-borne coronagraphic instruments like Roman-CGI and with ELTs around low-mass stars. In four experiments conducted with the ACE testbed, a range of different phase perturbations degraded the average intensity of the dark hole within a scoring region greater than $10 (\lambda/D)^2$ area by a factor of 13--26 and over the entire dark hole by up to a factor of 10. Spatial LDFC restores the average intensity of the entire dark hole to within a factor of 1.2--1.4 of its original contrast. In the scoring region focused on the perturbations, Spatial LDFC converges to within a factor of 1.2--1.7 of the original dark hole contrast and achieves a contrast gain of 10--13 within the scoring region. Spatial LDFC maintains the average dark hole contrast for over 100 iterations.

Though not strictly required as a part of Milestone 1, we also investigated the efficacy of spatial LDFC vs. standard DM probing methods for restoring a corrupted DH. Spatial LDFC shows significant potential advantages. When presented with the same aberrations, speckle nulling is able to achieve 25--40% deeper contrasts than LDFC. However, speckle nulling requires a factor of 2--5 more iterations to match Spatial LDFC's performance. As speckle nulling requires multiple modulations per iteration to estimate the phase of residual speckles in the DH, the duty cycle advantage for LDFC in terms of DM commands is substantial: a factor of 20--50 in our experiments.

Linear Dark Field Control may provide a promising path forward to maintain dark holes without relying on DM modulation and probing, especially if its small performance gap compared to probing techniques is closed and if possible null space can be mitigated.

The full duty cycle offered by LDFC improves the efficiency of high-contrast imaging observations.

By construction, LDFC drives the dark hole back to its initial state, which should improve the temporal correlation of speckles, while the LDFC loop is in operation. A full duty cycle and increased dark hole stability should substantially improve our ability to image mature solar system-like planets in reflected light over the next two decades.

Lessons Learned and Drawbacks

In our experiments, Spatial LDFC's main drawback is that it converges to a dark hole contrast a factor of 1.2--1.7 higher than in the pre-aberrated state: i.e. while our stated Milestone was completed, we have not strictly demonstrated that Spatial LDFC fully restores an aberrated DH. Experimental conditions may account for much of this performance gap. For example, laser centroid drift during the RM calculation may

compromise the accuracy of our influence function for LDFC. Drift during the closed-loop tests themselves likewise limits the accuracy of our correction. Instability in the laser power on the few percent level may limit accuracy as the average DH contrast approaches the initial, pre-aberrated state. The G-matrix encoding relationship between DM pokes and complex amplitudes for EFC may change with time, and similarly the RM for LDFC degrades with time.

Weak/bad actuators on the DM not currently flagged may lead to a poor influence function determination and impede convergence. This was a particular concern at ACE. Prior to our December experiments and immediately after tests of Multi-Star Wavefront Control, the DM at ACE began exhibiting significantly more bad/dead actuators. Some would flip polarity during various times between September 2019 and January 2020. Whether these bad/dead actuators resulted from the MSWFC tests in some way or simply reflect aging of the DM is unknown. Regardless, delays caused by the DM coupled with the COVID-19-induced shutdown of Ames did prevent additional laboratory tests seeking to improve our wavefront control look.

Some of the aberrations degrading the DH may produce intensity variations at/near lowest-flux regions of the bright field may lie also in a quadratic response regime. A region of the bright field in the quadratic response regime would preclude identifying a unique DM shape that could be applied to restore its initial state and that of the dark field. This is a particularly relevant possibility for the residual speckle core left in Experiment #4, as bright field region 180 deg from that speckle is at a local minimum in flux.

Laser drift can be better corrected by monitoring the centroid position during the RM calculation and by improving our loop speed. Better regularization can limit the impact of laser instability. Future Spatial LDFC experiments at ACE will be conducted with a repaired DM or a replacement free of bad/dead actuators and with a more efficient loop to reduce the impact of system RM evolution.

A key concern for future progress with Spatial LDFC is the existence of null space, where a given pupil-plane perturbation aberrates the dark field but produces a negligible change in the bright field. Null space is expected to include a combination of amplitude and phase errors, which can create single-side speckles. By construction, our experiments only demonstrated spatial LDFC's ability to remove phase errors that are represented by a linear combination of DM pokes (e.g. not perturbations with a spatial frequency higher than the DM pitch). More importantly, we did not, in this experiment, introduce amplitude errors in the pupil plane. It is expected that a combination of amplitude and phase errors can create single-sided speckles that are in the LDFC measurement null space. Amplitude errors can result from reflectivity variations in system optics and phase-induced errors due to out of plane optics. Amplitude errors are expected to be equally important at raw contrasts in the range of 10^{-7} -- 10^{-9} or below (e.g. Shaklan and Green 2006). A phase aberration induced speckles may also be in the linear measurement null space if its corresponding bright field twin falls on a dark

region of the bright field -- this effect may be the cause for the residual feature in Experiment #4.

Null space can be addressed in the following ways. To partially compensate for null space for Spatial LDFC, the bright field mask could be adjusted, adding pixels exterior to but on the same side as the dark field, to be sensitive to at least some amplitude errors. It may be possible to treat amplitude and high spatial frequency phase perturbations by solving for an aberration map informed by a regression procedure. Constructing such a map requires quantitative modeling of the DM and coronagraph optical train and will be the subject of future work in simulations and on the ACE testbed. Finally, spectral LDFC (Guyon et al. 2017) utilizing out-of-band measurements over the same focal plane region for the bright and dark fields, instead of different regions as in spatial LDFC, should be sensitive to both phase and amplitude aberrations provided that the main wavefront change is due to optical path difference in/near the pupil plane (where largest optics are). Improvements in the experimental setup for LDFC will enable better tests of the method's fundamental limits. Masking of lower-flux pixels with the bright field can focus LDFC on focal plane regions responding linearly to perturbations.

Future Work

Realistic aberrations (e.g. linear combination of Zernike modes) introduced mimicking those expected in flight for missions like Roman-CGI may provide a better practical test of Spatial LDFC. Our tests focus on sudden introductions of large-intensity perturbations into the dark field. An alternate test where smaller perturbations are periodically introduced and then corrected may better simulate closed-loop operations. Our experiments were conducted with the residual DH signal well illuminated. ``Blind" tests -- where the DH residual intensity is comparable to the detector noise level over the WFS sampling time -- can better assess LDFC's advantage over DM probing techniques in the (dark field) photon-starved regime. Adopting more advanced focal-plane wavefront sensing techniques such as EFC, Kalman filtering, or variants that optimize DM probing and integration time (e.g. Groff and Kasdin 2013) instead of speckle nulling may provide a more robust assessment of LDFC's advantages to state-of-the-art DM probing FPWFC methods.

Modal control will be implemented to optimize LDFC performance and allow for more in-depth analysis. For MS#1, we employed a sharp modal cutoff to compute the control matrix, with the number of modes controlled derived empirically to maintain control loop stability. A more powerful approach is to set a control gain for each control mode, and to measure control law performance (aberration rejection, noise level, stability condition) for each mode. Modal control is also required to optimally combine LDFC with other sensors in a full high contrast imaging system, and extrapolate close-loop performance in dynamical conditions with finite measurement sensitivity and temporal bandwidth.

Future work will include characterization of LDFC measurement null space, which is essential to:

- **Interpret laboratory results.** MS#1 results show that post-LDFC, the contrast does not return to the original contrast value. We suspect this is due to measurement null space: some modes are not measured by LDFC, so they cannot be corrected. In future work, we will track what part of incoming wavefront aberrations falls within the null space, so that the corresponding contrast term can be quantified in measured post-LDFC contrast.
- **Extrapolate LDFC performance to realistic conditions.** While our MS#1 tests injected pure OPD wavefront aberrations in the DM, a full high contrast imaging system will include a broader range of aberrations, including amplitude errors created by diffractive propagations of out-of-plane OPD aberrations. Extrapolation from lab results to on-orbit performance requires knowledge of optical system WF variations within LDFC's null space.
- **Understand how to deploy LDFC in a full wavefront control system.** LDFC will ultimately be combined with other wavefront sensors, such as a coronagraphic WFS measuring low-order modes. Spectral and spatial LDFC sensors may also be running concurrently on the same optical system. While this multi-sensor approach should be able to increase measurement completeness (reduced null space) and sensitivity, the associated wavefront control must have knowledge of all sensors' null spaces and modal sensitivity, such that the wavefront control law can adequately allocate control authority between sensor's input signals.

Modal control/analysis, together with null space measurement, will allow for LDFC performance to be extrapolated to realistic dynamical conditions. For each mode within LDFC's control space (outside the null space), modal analysis can quantify measurement sensitivity such that measurement noise can be computed as a function of bright field flux and exposure time. With knowledge of dynamical wavefront aberration timescales, the control law speed can then be optimized as a tradeoff between photon and readout noise propagation (reduced by slowing down the control loop) and temporal lag (reduced by speeding up the control loop). Future demonstrations will include dynamical tests to explore this tradeoff and validate associated control and analysis algorithms.

Upcoming/proposed NASA missions capable of imaging exoplanets in reflected light like Roman-CGI, HabEx, and LUVOIR require sustained raw contrasts of 10^{-9} -- 10^{-10} . Vacuum chamber experiments on the *High-Contrast Imaging Testbed* at the Jet Propulsion Laboratory will provide a first test of Linear Dark Field Control's efficacy at these extreme contrast regimes. For these tests, we will employ Spectral LDFC (Guyon et al. 2017), where out-of-band focal-plane images at wavelengths bracketing that of the main science bandpass will be needed to restore and freeze the dark hole.

Typical exposures for these missions will be several to tens of hours. A key milestone then will be to demonstrate stability at $< 10^{-9}$ -- 10^{-10} contrast for tens of hours.

Future Milestone Demonstrations within LDFC effort

The next milestone (MS2) will extend the current work to deeper contrast and demonstrate spectral LDFC. The current envisioned MS2 goal (pending formal approval by ExEp) is:

Demonstrate a 10x gain in raw contrast in the presence of injected disturbances by use of spectral LDFC stabilization in a dark hole with area covering at least 10 λ -I/D and reaching a raw contrast (post-LDFC) level below $1e-7$.

The higher contrast requirement will require a high-stability testbed, so we envision that this milestone will be demonstrated in a vacuum testbed at JPL. Wavelength diversity will be achieved by switching the light source alternatively between three wavelengths (dark hole wavelength + one wavelength on either side).

Beyond MS#2, further efforts and milestones will be aimed at improving contrast stability beyond the $1e-7$ goal, integration of spatial and spectral LDFC in a full high-contrast imaging system, and using LDFC telemetry toward post-processing contrast gains.

References

Bailey, V. P., Bottom, M., Cady, E., et al. 2018, in Society of Photo-Optical Instrumentation Engineers (SPIE) Conference Series, Vol. 10698, Proc. SPIE, 106986P

Borde, P. J., & Traub, W. A. 2006, ApJ, 638, 488

Cady, E., Prada, C. M., An, X., et al. 2016, Journal of Astronomical Telescopes, Instruments, and Systems, 2, 011004

Crill, B., Siegler, N., Bendek, E., Mamajek, E., & Stapelfeldt, K. 2019, in Bulletin of the American Astronomical Society, Vol. 51, 91

Currie, T., Pluzhnik, E., Guyon, et al., 2020, Publications of the Astronomical Society of the Pacific, 130, 104502

Groff, T., Kasdin, N. J., 2013, Journal of the Optical Society of America, 30, 128

Give'on, A., Kern, B., Shaklan, S., Moody, D. C., & Pueyo, L. 2007, in Society of Photo-Optical Instrumentation Engineers (SPIE) Conference Series, Vol. 6691, Proc. SPIE, 66910A

Guyon, O., Miller, K., Males, J., Belikov, R., & Kern, B., 2017, arXiv e-prints, arXiv:1706.07377

Guyon, O., Mazin, B., Fitzgerald, M., et al. 2018, in Society of Photo-Optical Instrumentation Engineers (SPIE) Conference Series, Vol. 10703, Adaptive Optics Systems VI, 107030Z

Males, J. R., & Guyon, O. 2018, Journal of Astronomical Telescopes, Instruments, and Systems, 4, 019001

Marois, C., Macintosh, B., Barman, T., et al. 2008, Science, 322, 1248

Miller, K., Guyon, O., & Males, J. 2017, Journal of Astronomical Telescopes, Instruments, and Systems, 3, 049002

N'Diaye, M., Dohlen, K., Fusco, T., & Paul, B. 2013, A&A, 555, A94

Shaklan, S., B., Green, J. J., ApOpt, 45, 5143